URSI GASS 2023, Sapporo, Japan, 19 – 26 August 2023

Device Placement Problem Analysis in General-Purpose Microwave Photonic Processors (GPMWPPs) Implemented using Barium Titanate Based Electro-optically Tunable Devices

Tushar Gaur*(1), Pragya Mishra(1), Talabattula Srinivas(1) and Gopalkrishna Hegde(2)
(1) Department of Electrical Communication Engineering, Indian Institute of Science, Bangalore, Karnataka, India - 560012
e-mail: tushargaur@iisc.ac.in, pragyamishra@iisc.ac.in, tsrinu@iisc.ac.in
(2) Department of Aerospace Engineering, Indian Institute of Science, Bangalore, Karnataka, India - 560012 e-mail: gopalkrishna@iisc.ac.in

Abstract

GPMWPP is a recent and innovative field for implementing parallel processing in photonic integrated circuits. Light distribution in these circuits is controlled via tunable MZIs using the thermo-optic effect which increases the dependencies on the high-performance blocks due to slower response time and smaller operational bandwidths. To address this limitation, GPMWPPs can be implemented using electro-optic effect offered by BTO devices. However, due to inherent anisotropy associated with BTO correct placement of devices, achieving identical performance for devices in various orientations becomes a challenge. In this work we propose a solution addressing the device placement problem in GPMWPP circuits.

1 Introduction

Similar to FPGA and multiprocessing cores in electronics enabling the implementation of multiple functionalities on the same chip, a paradigm shift from the application-specific photonic integrated circuit to reconfigurable general-purpose microwave purpose photonic processor (GPMWPP) have been observed in recent years [1]-[5]. GPMWPPs find wide-scale applications in civil, defence, aerospace and satellite operations, enabling the implementation of LiDARS, communications links (including modulator, filters, interrogators), high throughput biomedical sensing units, various photonic signal processing steps on the same reconfigurable circuit [1], [6], [7]. A GPMWPP consist of tunable directional couplers (implemented using MZIs for enhanced fabrication tolerance) waveguide mesh arranged in a specific geometry (triangular, rectangular or hexagonal) along with external high-performance blocks [5]. Light distribution in these circuits is governed by manipulating the phase in the branches of MZIs to reconfigure the circuit for implementing multiple functions simultaneously, thus enabling parallel processing. Given the advantages of hexagonal topology, a hexagonal architecture is utilized in the GPMWPPs [5]. However, the GPMWPPs demonstrated so far are tuned using the thermo-optic effect, which leads to heavy dependencies on high-performance blocks for implementing simple functions such as modulation, simple filters etc., due to slower response of thermo-optic tuning (5 μs - 200 μs).

To address this issue, GPMWP needs to be implemented using electro-optic tuning, which offers faster response time and higher bandwidths. However, the device size should be limited below 1 mm in these circuits to efficiently implement resonant architecture with large FSR and low insertion losses. Although lithium niobate on insulator is the most commonly used electro-optic platform for photonic integrated circuits today, but it can not be utilized directly for implementing GPMWPPs as it is limited by large device lengths (5 mm - 20 mm) [8], [9]. Device length can be reduced by increasing V_π, but it will result in high power consumption per 180^o phase shift and other nonlinear effects coming into play. Another method to reduce device length is to utilize material platforms offering higher Pockel's coefficient and being CMOS compatible. Barium Titanate (BTO) is a ferroelectric material which stays in a centrosymmetric cubic structure above the curie temperature of 120^{o}C, where it does not possess any linear Pockel's effect. However, below Curie temperature, the crystal changes to tetragonal structure with c lattice parameter stretched compared to shrinked 'a' and 'b' parameters (a=b) and offers the largest Pockel's coefficient which is nearly 30 times the largest Pockel's coefficient offered by lithium niobate [10]-[12]. Due to ferroelectric behaviour, BTO possesses instantaneous polarization aligned along the c-axis. While film growth, the polarization domains are created in 4 orthogonal directions as shown in Figure 1. However, on applying a static electric field in the form of voltage bias, the polarizations are arranged in the same direction parallel to the c-axis. Since a hexagonal topology is being

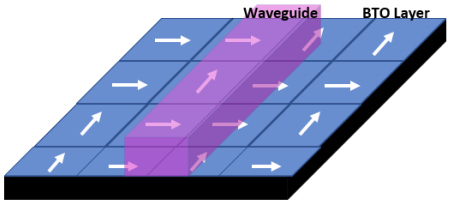

Figure 1. Two orthagonal domain formation in a-axis oriented BTO layer.

utilized for establishing the architecture of GPMWPPs, the devices exist in 3 orientations (0, θ and $-\theta$), where θ is the angle of the slanted edge of the hexagon. Since BTO is an anisotropic material, the device performance will vary with the change in orientation of the device due to a change in effective Pockel's coefficient. This opens up the challenge of device placement in GPMWPP architecture. For efficient operation of GPMWPPs, the devices in the three orientations must perform identically. With the maturity in fabrication technology and accurate design technology, it is possible to reliably predict the correct placement of devices in GPMWPPs such that the devices in three orientations offer identical operation bandwidth and $V_\pi L$ (these are also known as FOM for MZIs). Thus, in this work, we analyze the effect of varying orientation angles on effective Pockel's coefficient in detail and propose an optimized solution for the device placement challenge in electro-optically tuned GPMWPPs.

2 Theoretical Background

2.1 Device Structure

The proposed device structure utilizes coplanar waveguide electrodes in a push-pull configuration on an a-oriented BTO (c-axis in the plane of the device's top view) on the SOI hybrid platform. An a-oriented BTO layer of thickness 0.1 μm over Si layer of 0.1 μm on SiO_2 buried oxide layer of 4.7 μm is considered. The rib of amorphous silicon is considered for light confinement and propagation. RF field is applied using gold electrodes deposited on BTO directly. A cladding of SiO_2 is also provided to allow micro vias connections and safeguard the device against environmental damage. The device structure is shown in Figure 2.

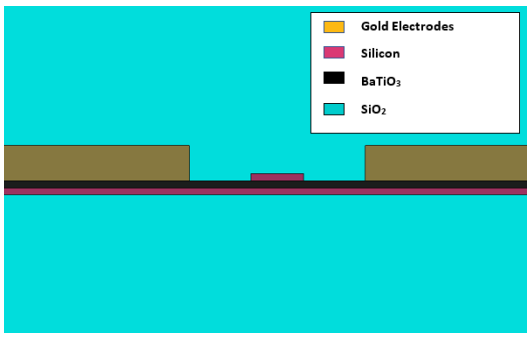

Figure 2. Cross section view of the device proposed

Table 1. Dimensions of various layers in Device

t_{Au}	w_c	w_g	w_{rib}	t_{clad}
0.5 μm	8.25 μm	2.5 μm	0.75 μm	3 μm

Dimensions of various layers and parameters in Figure 2 are summarized in Table 1. Here t_{Au}, w_c, w_g and t_{clad} are

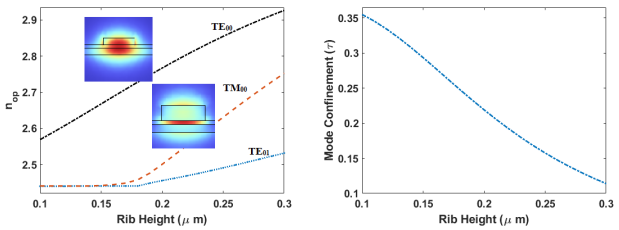

(a) **(b)**

Figure 3. (a)Dispersion curve and (b) Light confinement dactor (τ) in BTO for varying rib height h_{rib}.

electrode thickness, trace electrode width, electrode gaps and cladding thickness. Rib height decides the number of propagation modes and light confinement factor within the BTO. Since silicon does not have its own electro-optic effect, the phase shift on the application of RF field occurs only due to the light confined within the BTO layer. To analyze the effects of varying h_{rib}, the dispersion curve and light confinement factor in BTO are plotted in Figure 3a and 3b, respectively. The figure depicts that for a single mode operation h_{rib} should be kept below 0.17 μm and the mode confinement factor reduces as the rib height increases.

2.2 Effect of Device Orientation

Since BTO is an anisotropic material, with spontaneous polarization along c-axis its electro-optic performance can be modelled using index ellipsoid equation given by:

$$\left(\frac{1}{n_o^2}+r_{13}E_z\right)x^2+\left(\frac{1}{n_o^2}+r_{13}E_z\right)y^2+\left(\frac{1}{n_e^2}+r_{33}E_z\right)z^2 +2(r_{51}E_y)yz+2(r_{51}E_x)xz=1 \quad (1)$$

Here n_e and n_o are extraordinary and ordinary refractive index of BTO whose values are calculated using Sellmeier Equation (n_e=2.27 and n_o=2.3) and r_{mn} represents the Pockel's coefficient. Since BTO has 4mm space group its Pockel's coefficient tensor is given as:

$$\begin{bmatrix} 0 & 0 & r_{13} \\ 0 & 0 & r_{13} \\ 0 & 0 & r_{33} \\ 0 & r_{42} & 0 \\ r_{51} & 0 & 0 \\ 0 & 0 & 0 \end{bmatrix} \quad (2)$$

Here r_{13}= 8 pm/V, r_{33} = 28 pm/V and r_{42} = r_{51} = 800 pm/V [**?**]. For an a-oriented BTO device if electric field is applied along z-axis, the electro-optic performance will be determined by r_{33}. However, if the device is rotated by an angle ϕ, then the index ellepsoid will follow rotated coordinates given by:

$$x = x'cos(\phi)+z'sin(\phi) \quad (3a)$$

$$z = -x' sin(\phi) + z' cos(\phi) \quad (3b)$$

Substituting equations (3a) and (3b) in equation (1):

$$\left(\frac{1}{n_o^2} + r_{13}E_{z'}cos(\phi)\right) z'^2 sin^2(\phi) + \left(\frac{1}{n_e^2} + r_{33}E_{z'}cos(\phi)\right) \times z'^2 cos^2(\phi) + 2(r_{51}sin(\phi)E_{z'})z'^2 sin(\phi)cos(\phi) = 1 \quad (4)$$

From the above equation effective Pockel's coeffiecient as a function of roatation angle ϕ can be given as:

$$r_{eff}(\phi) = r_{33}cos^3(\phi) + (2r_{51} + r_{13})sin^2(\phi)cos(\phi) \quad (5)$$

Refractive index for rotated cordinates is given by:

$$n_{z'}(\phi) = \frac{n_o n_e}{\sqrt{n_o cos^2(\phi) + n_e sin^2(\phi)}} \quad (6)$$

Since BTO is a ferroelectric material with certain spontaneous polarization which will be oriented in 4 orthagonal direction, above equation are valid only if all the domains are oriented along c-axis. However, considering two domains 0° and 90° are present in the waveguide region then above equations for effective Pockel's coefficient and refractive index are modified to:

$$r'_{eff}(\phi, \alpha) = (1-\alpha)r_{eff}(\phi) + \alpha r_{eff}(90-\phi) \quad (7)$$

$$n'_{z'}(\phi, \alpha) = (1-\alpha)n_{z'}(\phi) + \alpha n_{z'}(90-\phi) \quad (8)$$

here α represents the polarization factor. For considering all the possible domains the same equation can be modified with four polarization factors.

3 Results and Discussions

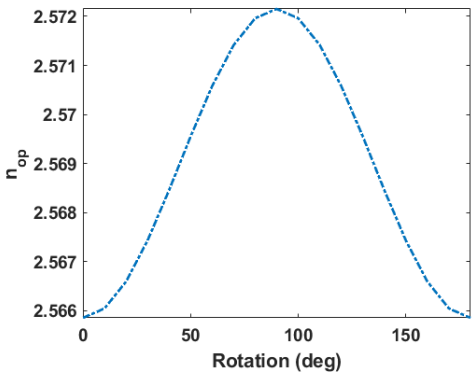

Figure 4. Effective mode index n_{op} versus roataion angle.

Based on results obtained in Figure 3 h_{rib} is decided to be 0.1 μm to attain single mode operation while maintaining a high confinement factor of $\tau = 0.35$. Using these values optical mode profile was calculated (TE_{00} and TM_{00} mode profiles are plotted in the inset of Figure 3). However, due to the inherent anisotropy of BTO, the mode index will vary with the device's orientation. T_{00} mode index against varying rotation angle is plotted in Figure 4. The figure shows that the optical mode index increases with rotation angle till 90° and then decreases. This value is vital in calculating the phase shift due to the applied field for the device.

Since the expected device size is smaller than 1 mm, lumped electrodes are considered and RF response is calculated using a commercial FEM solver for varying RF frequency, and depicted in Figure 5. For the purpose of RF simulation BTO's dielectric constant is taken to be 1200 and 56 along a-axis and c-axis, respectively [13]. Figure 5a depicts the S_{21} response of the device from which the 3 dB RF bandwidth is calculated to be 46 GHz, and S_{11} response is shown in Figure 5b. The figure depicts S_{11} for the device remains fairly low, thus ensuring efficient power delivery to the electrodes. Changes in RF characteristics of the device with changing orientation were found negligible.

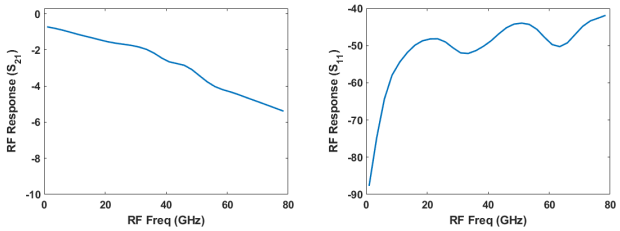

Figure 5. RF responses (a)S_{21} and (b) S_{11} for the proposed device.

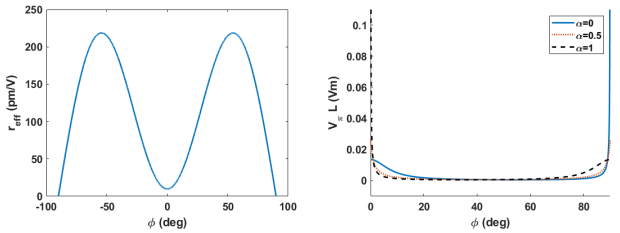

Figure 6. (a) Effective pockel's coefficient (r_{eff}) and (b) $V_\pi L$ for different polarization factors (α) versus orientation angle.

The electro-optic effect is applicable only in the BTO layer; thus, the confinement factor calculated in Figure 3 plays a significant role in determining the electro-optic performance of the device and limits the maximum possible r_{eff} to $r_{effmax} = \tau \times r_{51}$ = 280p pm/V. To analyze the electro-optic response, effective Pockel's coefficient is calculated for varying device orientations and plotted in Figure 6a. The figure shows th at the maximum effective Pockel's coefficient of 218.53 pm/V is obtained at 54° orientation for single domain device. For a push-pull configuration, the applied field in the second branch of the MZI will be 180° rotated compared to the field in the first branch; thus, the magnitude of r_{eff} remains the same with the opposite phase.

Thus V_πL is given using equations (6), (7) and (8) as:

$$V_\pi L = \frac{\lambda w_g}{2\tau n_{z'}^{'3}(\phi,\alpha) r'_{eff}(\phi,\alpha)} \tag{9}$$

Using equation (9), $V_\pi L$ is plotted against varying orientations for different polarization factors in Figure 6b. From the figure, it can be observed that V_πL remains constant for most of the orientation range for all the polarization factors, which ensures that by changing polarization factor, V_πL is not affected for different device orientations.

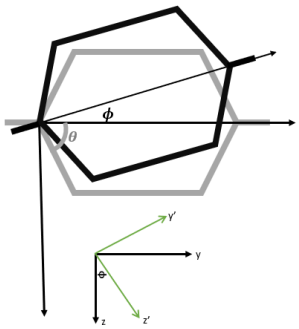

Figure 7. Unit hexagonal cell optimized geometry.

4 Conclusion

Since in a hexagonal GPMWPP we encounter three device orientations (0^o, θ and $-\theta$), it is essential to select the parameters ϕ and θ such that all the devices in the three orientation perform equally in terms of r_{eff}. In order to find optimum placement for the hexagonal architecture GPMWPPs, an optimization is run across the values obtained in Figure 6a to find three equally spaced angles at which r_{eff} remain the same. Three angles obtained after optimization was 26^o, 78^o and -26^o, at these angles r_{eff} were found to be 105 pm/V and results in Figure 6b it is ensured that the V_πL at the obtained angles remain same. This means that the hexagon cell has slanted branches at angle -56^o and 56^o, and then the whole geometry is rotated by 26^o giving rise to three orientations $26^o, 78^o$ and -26^o as shown in Figure 7.

Acknowledgements

We would like to thank Ministry of Education, Government of India, for funding this research under Prime Minister's Research Fellowship scheme.

References

[1] Leimeng Zhuang, Chris G. H. Roeloffzen, Marcel Hoekman, Klaus-J. Boller, and Arthur J. Lowery, "Programmable photonic signal processor chip for radiofrequency applications", Optica 2, pp. 854-859, 2015.

[2] Daniel P´erez, Ivana Gasulla, Prometheus Das Mahapatra, and Jos´e Capmany, "Principles, fundamentals, and applications of programmable integrated photonics", Adv. Opt. Photon. 12, pp. 709-786, (2020).

[3] M. Teng et al., "Miniaturized Silicon Photonics Devices for Integrated Optical Signal Processors", Journal of Lightwave Technology, vol. 38, no. 1, pp. 6-17, (2020).

[4] David A. B. Miller, "Perfect optics with imperfect components", Optica 2, pp. 747-750, (2015).

[5] D. P. Lopez, Ivana Gasulla, Jos´e Capmany, and Richard A. Soref, "Reconfigurable lattice mesh designs for programmable photonic processors," Opt. Express 24, pp. 12093-12106, (2016).

[6] Aitor L´opez, Daniel P´erez, Prometheus DasMahapatra, and Jos´e Capmany, "Auto-routing algorithm for field-programmable photonic gate arrays", Opt. Express 28, pp. 737-752 (2020).

[7] Xingwei Ye, Fangzheng Zhang, and Shilong Pan, "Optical true time delay unit for multi-beamforming," Opt. Express 23, pp. 10002-10008, (2015).

[8] Abu Naim R. Ahmed, Shouyuan Shi, Andrew Mercante, Sean Nelan, Peng Yao, and DennisW. Prather, "High-efficiency lithium niobate modulator for K band operation", APL Photonics 5, 091302 (2020).

[9] Ashutosh Rao, Aniket Patil, Payam Rabiei, Amirmahdi Honardoost, Richard DeSalvo, Arthur Paolella, and Sasan Fathpour, "High-performance and linear thin-film lithium niobate Mach–Zehnder modulators on silicon up to 50 GHz", Opt. Lett. 41, pp. 5700-5703 (2016).

[10] Girouard, P. D., Chen, P., Jeong, Y. K., Liu, Z., Ho, S-T. and Wessels, B. W., "X-(2) Modulator With 40-GHz Modulation Utilizing BaTiO3 Photonic Crystal Waveguides". IEEE Journal of Quantum Electronics, 53(4), (2017).

[11] Geler-Kremer, J., Eltes, F., Stark, P. et al. A ferroelectric multilevel non-volatile photonic phase shifter. Nat. Photon. 16, 491–497 (2022).

[12] Pau Castera, Ana M. Gutierrez, Domenico Tulli, Sébastien Cueff, Regis Orobtchouk, Pedro Rojo Romeo, Guillaume Saint-Girons and Pablo Sanchis, "Electro-Optical Modulation Based on Pockels Effect in BaTiO3 With a Multi-Domain Structure", IEEE Photonics Technology letters, vol. 28, no. 9, (2016)

[13] Alvaro Rosa, Domenico Tulli, Pau Castera, Ana M. Gutierrez, Amadeu Griol, Mariano Baquero, Bertrand Vilquin, Felix Eltes, Stefan Abel, Jean Fompeyrine, and Pablo Sanchis, "Barium titanate (BaTiO3) RF characterization for application in electro-optic modulators," Opt. Mater. Express 7, pp. 4328-4336, (2017).